

# How Far Can We Get with Neural Networks Straight from JPEG?

Samuel Felipe dos Santos, Nicu Sebe, and Jurandy Almeida

**Abstract**—Convolutional neural networks (CNNs) have achieved astonishing advances over the past decade, defining state-of-the-art in several computer vision tasks. CNNs are capable of learning robust representations of the data directly from the RGB pixels. However, most image data are usually available in compressed format, from which the JPEG is the most widely used due to transmission and storage purposes demanding a preliminary decoding process that have a high computational load and memory usage. For this reason, deep learning methods capable of learning directly from the compressed domain have been gaining attention in recent years. These methods adapt typical CNNs to work on the compressed domain, but the common architectural modifications lead to an increase in computational complexity and the number of parameters. In this paper, we investigate the usage of CNNs that are designed to work directly with the DCT coefficients available in JPEG compressed images, proposing a handcrafted and data-driven techniques for reducing the computational complexity and the number of parameters for these models in order to keep their computational cost similar to their RGB baselines. We make initial ablation studies on a subset of ImageNet in order to analyse the impact of different frequency ranges, image resolution, JPEG quality and classification task difficulty on the performance of the models. Then, we evaluate the models on the complete ImageNet dataset. Our results indicate that DCT models are capable of obtaining good performance, and that it is possible to reduce the computational complexity and the number of parameters from these models while retaining a similar classification accuracy through the use of our proposed techniques.

**Index Terms**—Deep Learning, Convolutional Neural Network, Computational Efficiency, Compressed-Domain Processing, Computer Vision.

## I. INTRODUCTION

Convolutional neural networks (CNNs) have brought astonishing advances in computer vision, being used in several application domains, such as medical imaging, autonomous driving, road surveillance, and many others [1], [2].

However, in order to increase the performance of these methods, increasingly deeper architectures have been used, leading to models that consume a great amount of memory and demand a high computation cost for inference [3].

For this reason, in spite of all the advances, the computational cost is still one of the main problems faced by deep learning architectures [4]. The significant amount of model

Samuel Felipe dos Santos and Jurandy Almeida are with the Instituto de Ciéncia e Tecnologia, Universidade Federal de São Paulo – UNIFESP, 12247-014, São José dos Campos, SP – Brazil, e-mail: {felipe.samuel, jurandy.almeida}@unifesp.br.

Nicu Sebe is with the Dept. of Information Engineering and Computer Science, University of Trento – UniTn, 38123, Trento, TN – Italy, e-mail: niculae.sebe@unitn.it.

Manuscript received April 19, 2005; revised August 26, 2015.

parameters to be stored and the high GPU processing power needed for using such models can prevent their deployment in computationally limited devices, like mobile phones and embed devices [5]. Therefore, specialized optimizations at both software and hardware levels are an imperative need for developing efficient and effective deep learning-based solutions [6].

For storage and transmission purposes, most image data available are often stored in a compressed format, like JPEG, PNG and GIF [7]. From these formats, JPEG has remained the most popular despite the advances in video compression and is considered a simple solution to store and transmit visual data [8]. To use this data with a typical CNN, it would be required to decode it to obtain the RGB images used as input, a task demanding high memory and computational cost [1].

A possible alternative to alleviate this problem is to design CNNs capable of learning with DCT coefficients rather than RGB pixels [1], [4], [7], [8], [9], [10], [11], [12], [13], [14]. The DCT is a representation of the data in the frequency domain that can be easily extracted by partial decoding, saving computational cost. Frequency domain image processing can yield advantages like computational efficiency and spatial redundancy removal, being used successfully in many computer vision tasks, like image compression, image coding, signature verification, gender classification, face recognition, human gait recognition, among others [15].

In this paper, we evaluate the potential of CNNs designed for the compressed domain, taking into account not only the classification accuracy, but also the computational efficiency of the models. For this study, we consider a state-of-the-art CNN recently proposed by Gueguen et al. [9], which is a modified version of the ResNet-50 architecture [16]. Despite the speed-up obtained by partially decoding compressed data, the changes lead to a significant decrease in its computational efficiency. To alleviate its computational complexity and number of parameters, we extended the network of Gueguen et al. [9] to include a handcrafted and data-driven techniques for reducing the amount of input channels that are fed to the network.

Extensive experiments were conducted, starting with ablation studies on a subset of ImageNet, analysing the effects of different frequency ranges, image resolution, JPEG quality and classification difficulty. Then, we conduct experiments on the complete ImageNet dataset. The reported results indicate that neural networks designed to work directly on the frequency domain with DCT coefficients can achieve performance comparable to other baseline methods. By using our handcrafted and data-driven strategies to learn how to reduce the amount

of input channels, we were able to reduce the computational complexity of such networks, making them faster than the RGB baseline.

A preliminary version of this work was presented at IEEE International Conference on Image Processing (ICIP 2020) [17]. Here, we introduce several innovations. First, we present an in-depth review of deep learning methods that take advantage of the JPEG compressed domain. In addition, we discuss new strategies for reducing the amount of input channels that are fed to the network. Moreover, we conduct an extensive experimental evaluation on a much larger and on a more challenging dataset and report new experiments both for the analysis of the evaluated methods and for the comparison with other works. Finally, we also include a performance analysis of different models regarding their network inference speed in terms of frames per second (FPS), considering both the data preprocessing time and the network time.

The remainder of this paper is organized as follows. Section II briefly reviews the JPEG image compression algorithms. Section III discusses related work. Section IV describes our approach to reduce the computational cost for decoding images by training CNNs directly on the compressed data. Section VI presents the experimental setup and reports our results. Finally, we offer our conclusions and directions for future work in Section VII.

## II. JPEG COMPRESSION

The JPEG standard (ISO/IEC 10918) was created in 1992 and is currently the most widely-used image coding technology for lossy compression of digital images. The basic steps of the JPEG compression algorithm are presented in Figure 1.

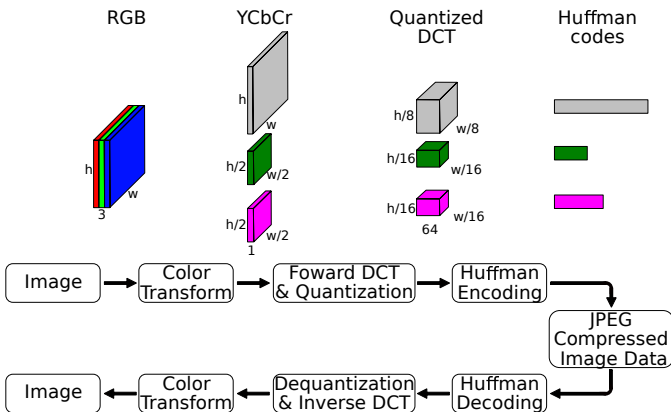


Fig. 1. JPEG compression and decompression process [9].

Initially, the representation of the colors in the image is converted from RGB to YCbCr, which is composed of one luminance component (Y), representing the brightness, and two chrominance components, Cb and Cr, representing the color. Also, the Cb and Cr components are down-sampled horizontally and vertically by a factor of 2, as human vision is more sensitive to brightness details than to color details. Then, each of the three components is partitioned into blocks of 8x8 pixels and 128 is subtracted from all the pixel values. Next, each block is converted to a frequency domain representation by the forward discrete cosine transform (DCT).

The result is an 8x8 block of frequency coefficient values, each corresponding to the respective DCT basis functions, with the zero-frequency coefficient (DC term) in the upper left and increasing in frequency to the right and down. The amplitudes of the frequency coefficients are quantized by dividing each coefficient by a respective quantization value defined in quantization tables, followed by rounding the result to the nearest integer. High-frequency coefficients are approximated more coarsely than low-frequency coefficients, as human vision is fairly good at seeing small variations in color or brightness over large areas, but fails to distinguish the exact strength of high-frequency brightness variations. The quality setting of the encoder affects the extent to which the resolution of each frequency component is reduced. If an excessively low-quality setting is used, most high-frequency coefficients are reduced to zero and thus discarded altogether. To improve the compression ratio, the quantized blocks are arranged into a zig-zag order and then coded by the run-length encoding (RLE) algorithm. Finally, the resulting data for all 8x8 blocks are further compressed with a lossless algorithm, a variant of Huffman encoding. For decompression, inverse transforms of the same steps are applied in reverse order. If the DCT computation is performed with sufficiently high precision, quantization and subsampling are the only lossy operations whereas the others are lossless, therefore they are reversible.

## III. RELATED WORK

The processing of compressed data has been widely-explored by many conventional image and video processing techniques as an alternative to speed up the computation performance in a variety of applications, such as face recognition [18], image indexing and retrieval [19], saliency detection and image retargeting [20], video copy detection [21], video summarization [22], and many others.

In the deep learning era, the potential of the JPEG compressed domain for neural networks has received limited attention and a few works have emerged only recently. The key idea exploited by such works consists in adapting traditional CNN architectures to facilitate the learning with DCT coefficients rather than RGB pixels.

In this section we present a literature review of deep learning methods that use DCT coefficients. We divided such works into two categories according to how they are related to our approach: (1) works that aim to improve performance of CNNs by using information from the frequency domain, like DCT coefficients and (2) works that focus on deep model designed to process data directly from the frequency domain in the form of DCT coefficients.

In the first category, we can highlight the works of Ehrlich et al. [8], [12] that focus on two tasks with JPEG images: (i) artefact correction and (ii) the use of different quality settings.

The artifact correction task aims to restore information lost due to lossy compression methods. Although it has been well explored in the context of deep learning, the models are usually designed for a single JPEG quality level, limiting their

application on real world settings [12]. Ehrlich et al. [12] proposed a novel single model that is capable of dealing with variable levels of JPEG quality, called Quantization Guided JPEG Artifact Correction (QGAC). This is achieved by parameterizing the CNN with the quantization matrix of the JPEG images with the Convolutional Filter Manifold (CFM). Also proposed by Ehrlich et al. [12], the CFM is a variation of the Filter Manifolds, and uses a three layers CNN to output a convolutional kernel thought the quantization matrix, this way, it is possible to adapt the weights and bias according to JPEG quality level. The CFM works entirely on the frequency domain thought the DCT coefficients. Two subnetworks are used to process the data from the DCT coefficients. The BlockNet, that uses  $8 \times 8$  convolution and transposed convolution with stride 8, computing the representation of each DCT coefficient block separately. The weight of these layers are generated on inference time by CFM networks. The FrequencyNet rearrange the DCT coefficients using the FCR technique, learning per-frequency weights. Both subnetworks uses the Residual-in-Residual Dense Blocks (RRDB) [23] on their core. In order to artifact correct the Y color channel, the coefficients are feed to a BlockNet. Then the output goes thought the FrequencyNet and finally, another BlockNet. The output of the three subnetworks are concatenated and goes thought a fusion network. The resulting output is a residual that is added to the Y color channel in order to restore it. The artifact correction on the Cb And Cr color channels is made by independent networks for each channel. These networks also use the restored Y channel as input, since it has a greater resolution, presenting a smaller loss of information. These independent networks uses  $8 \times 8$  stride 8 convolutions and transposed convolutions with weights generated by CFMs as well as RRDBs. The output is a residual that is added to the Cb or Cr channel upsampled with Nearest Neighbor in order to restore it. In order to train the network, a loss function combining L1 error and Structural Similarity (SSIM) [24] is used. The resulting network is also fine-tuned with a GAN loss in order to restore texture in blurred regions, combining the L1 loss, the relativistic average GAN loss and a texture loss that is L1 distance between intermediate layer of the network.

There has been little study on the effect of the compression on deep learning methods, since most of the benchmark datasets contain JPEG compressed images with high quality, not representative of the quality level usually seen in consumer applications [8]. Ehrlich et al. [8] proposed a novel method called Task-Target Artifact Correction in order to mitigate the performance penalty of using JPEG images with not ideal compression qualities. The proposed method uses the QGAC [12] network to correct artifacts in the JPEG image before feeding them to the network. The novelty of the method is the fine-tuning of the artifact correction network in a unsupervised manner, using the L1 distance between the logits of the networks feed with compressed and uncompressed images. The method proved to be effective in recuperating the accuracy of the network, surpassing the performance from the base QGAC method and obtaining similar performance from the fine-tuning of the entire network on compressed images, while retaining the performance on the uncompressed images

and not requiring labeled data. Although the Task-Target Artifact Correction is effective and can be more easily applied to real word application due to been an unsupervised method, there is a considerable performance drop when compared with other methods [8].

On the second category, we highlight the works of Ehrlich and Davis [4], Lo et al. [10], Xu et al. [11], Gueguen et al. [9] and Deguerre et al. [1], [7], that use CNN with modifications designed specifically to deal with DCT coefficients and have architectures that can be used on multiple computer vision task with few modifications.

Ehrlich and Davis [4] reformulated the ResNet architecture to perform its operations directly on the JPEG compressed domain. Since the lossless operations used by the JPEG compression algorithm are linear, they can be composed along with other linear operations and then applied to the network weights. In this way, the basic operations used in the ResNet architecture, like convolution, batch normalization, etc, were adapted to operate in the JPEG compressed domain. For the ReLU activation, which is non-linear, an approximation function was developed.

In a different direction, Lo et al. [10] explore the task of semantic segmentation directly on the DCT representation of the images. The proposed method uses the Frequency Component Rearrangement (FCR) technique to code the relationship between the DCT coefficients in a new dimension, feeding them to the proposed DCT-EDANet, a version of the EDANet [25] architecture modified to operate on the frequency domain. The location of each DCT coefficient in a  $8 \times 8$  block represent its frequency index, for this reason, when a convolution is performed, the frequency relationship is misinterpreted as spatial relationship, failing to extract essential features [10]. The FCR technique used rearrange the DCT coefficients, separating the frequencies channel wise in a new dimension. All the frequency relationships are exclusively represented on this dimension, allowing for the proper use of 2D convolution on the DCT representation. Due to the smaller spatial resolution of the DCT representation, the downsampling operations usually applied in CNNs would lead to feature maps that are too small, losing spatial information and boundary details, crucial aspects for localizing objects [10]. For this reason, the DCT-EDANet removes all three downsampling blocks from the original EDANet, using a initial layer with a  $3 \times 3$  convolution, batch normalization and ReLU activation instead. The smaller spatial resolution of the DCT allow for the increase in depth of the network. DCT-EDANet have 22 EDA modules, while the original EDANet have 12, both having similar computational complexity. The DCT-EDANet obtained similar accuracy to the RGB baseline and was also able to reduce the amount of coefficient feed to the network to 36% of the lowest frequency components, indicating that the best proportion of Y, CB and Cr coefficients is approximately 50:25:25.

Xu et al. [11] proposed a method that can be applied to deep models with few modifications to the architecture in order to use information from higher resolution images, mitigating the loss of salient information caused by downsampling. The method consists of extracting the DCT coefficients of the image in order to obtain a representation on frequency domain,

followed by a training process where the network learns to dynamically select only a subset of the most relevant frequencies jointly with the task. In order to learn how to select frequency channels from the DCT input, a dynamic gate module is used. The original input goes through a average pooling layer, followed by a  $1 \times 1$  convolution. A multiplication by two trainable parameters is then applied, obtaining two values for each channel that represents the probability each channel being on or off. The Gumbel Softmax trick [26], [27], [28] is used in order to sample the probability values into 0s and 1s while allowing for back propagation. Finally, a point wise multiplication is used between the output of the dynamic gate model and the DCT coefficients.

To accelerate the training and inference speed, Gueguen et al. [9] proposed different architectural modifications to apply to the ResNet-50 network [16] in order to accommodate DCT coefficients from JPEG images and operate directly in the frequency domain. These coefficients can be obtained by partial decoding, thus saving the high computational load and memory usage in full decoding the JPEG images. The modifications made to accommodate the DCT consisted of skipping the first stage of the ResNet-50 network and alterations to the early blocks of the second and third stages to mimic the increase in receptive fields and stride of the baseline RGB model, calling this model Receptive Field Aware (RFA). In order to deal with the lower resolution of the Cb and Cr components, multiple methods were proposed. The Upsampling-RFA upsample the Cb and Cr components to match the resolution of the Y component and the Deconvolution-RFA do the same process, but with a deconvolution layer instead. On the Late Concat RFA (LC-RFA), the Y component goes through the modified versions of the first three stages of the network, while the Cb and Cr components go through a separate convolution block. Then, all components are concatenated and fed to the fourth stage. Gueguen et al. [9] also proposed the LC-RFA-Thinner, a version of the LC-RFA with altered number of channels on the first three convolution blocks that the Y component goes through, respectively, from 1024, 512, 512 channels, to 384, 384, 768.

Similarly, Deguerre et al. [1] proposed a fast object detection method which takes advantage of the JPEG compressed domain. For this, the Single Shot MultiBox Detector (SSD) [29] architecture was adapted to accommodate block-wise DCT coefficients as input. To preserve the spatial information of the original image, the first three blocks of the SSD network were replaced by a convolutional layer with a filter size of  $8 \times 8$  and a stride of 8. In this way, each  $8 \times 8$  block from JPEG compressed data is mapped into a single position in the feature maps used as input for the next layer. Deguerre et al. [7] also extended their aforementioned work by taking in consideration the sub-sampling of the chrominance problem and by also using the LC-RFA, Deconvolution-RFA and LC-RFA-Thinner networks from Gueguen et al. [9] as backbone to the SSD architecture, that originally used the VGG-16, naming them SSD300. Versions of the network with only the Y color channel were also tested, avoiding the learning impediments that may occur due to resolution and sparsity, while also

reducing bandwidth for image transfer. Experimental results showed that the use of the ResNet-50 modified for DCT coefficients performed better than the VGG-16, and that the performance obtained by only using the Y input was similar to the networks using YCbCr.

There are also other recent works that use information from the compressed domain but do not fit in such categories. Some of them rely on other types of information available in the JPEG compressed data, for instance, quantization tables. Other works have focused in a particular domain, allowing them to take advantage of prior knowledge of the domain and reduce levels of ambiguity when analysing the content of an image. For instance, Li et al. [30] performed artefact removal on JPEG images with multiple quality settings but used only quantization tables from the JPEG compressed data; Chen et al. [31] designed a network for video super-resolution using partition maps and motion vectors; Tang et al. [15] used a network designed for frequency data for facial expression recognition, however the DCT coefficients are not extracted from the JPEG compressed data, instead they are calculated from the decompressed images; and Qin et al. [32] proposed the FcaNet, a model that uses frequency channel attention, which selects and learns the best DCT bases to compress the input data, generating scalars that are used to weight the importance of each input channel.

For the category of CNN designed specifically for DCT coefficients, some works have been proposed recently, as the ones mentioned so far, but in general they have only focused on improving the effectiveness of a given model. When analysing models designed for DCT coefficients, it is also very important to take into account their efficiency, since one of their main advantages is the speed up obtained by partially decoding the images, but in order to increase accuracy, many works end up increasing the complexity of the model, losing this advantage. In spite of all the advances in this nascent area, a more comprehensive study considering efficiency aspects, such as computational complexity and number of parameters, is still missing.

This paper aims to fill such a gap. Here, we present a comprehensive study of DCT based models that considers not only their effectiveness but also their efficiency, such as computational complexity, number of parameters, and inference time. In addition, we propose different strategies to reduce the computational complexity and number of parameters of such models, in order to keep them similar to their RGB baselines.

#### IV. LEARNING FROM THE COMPRESSED DOMAIN

The DCT computation of a  $8 \times 8$  pixel block requires 1920 floating point operations (FLOPs) [33]. Although it seems negligible, computer vision tasks usually involve the processing of a great amount of images, each one containing many pixel blocks, therefore the total computational cost may be significant. Roughly speaking, the DCT can be seen as a convolution with a specific filter size of  $8 \times 8$ , stride of  $8 \times 8$ , one input channel, 64 output channels, and specific, non-learned orthonormal filters. As both the filter size and stride are equal to 8, spatial information of adjacent blocks

do not overlap. In theory, a standard convolutional layer may learn to behave like a DCT, but in practice, this is not trivial, as the learned bases may be undercomplete, complete but not orthogonal, or overcomplete. In spite of that, the use of DCT weights as input for a CNN is feasible, since they can be seen as the outputs of a convolution layer with frozen weights initialized from the DCT filters [9].

Motivated by the aforesaid observations, we examine ways of integrating frequency domain information into CNNs. To present date, little work has been done to exploit the DCT representation widely used in compressed data as input for neural networks [9].

The starting point for our proposal were the models from Gueguen et al. [9], which are adapted to facilitate the learning with DCT coefficients rather than RGB pixels. Between the different models proposed, we decided to focus on the Upsampling-RFA, since it had the second best top-1 error and the third best FPS, showing to be an efficient model [9].

On the Upsampling-RFA, DCT coefficients obtained from the Cb and Cr components are upsampled in order to match the resolution of the Y component. Then, the three components are concatenated channel-wise, passed through a batch normalization layer, and fed to the convolution block of the second stage of the ResNet-50 network. The second and third stages of the ResNet-50 network were changed to accommodate the amount of input channels and to ensure that the number of output channels at the end of these stages is the same of the original ResNet-50 network. Due to the smaller spatial resolution of the DCT inputs, early blocks of the second stage of the ResNet-50 network were altered to have a smoother increase of their receptive fields and, for this reason, their strides were decreased in order to mimic the increase in size of the receptive fields in the original ResNet-50 network.

These changes in the ResNet-50 network raised its computation complexity and number of parameters. In this way, although there was a the speed-up by partially decoding the images, there was also an increase in the computational cost for passing them through the network once they are loaded in memory. Also, the increase in the amount of parameters indicates that in order to reach a similar classification accuracy from the RGB model, the Upsampling-RFA needed to use a more robust model than the original.

Motivated by the above observations, we examine different ways of dealing with those issues. Our objective was to obtain a model that works directly on DCT coefficients, but also have a similar amount of parameters and computational complexity from the original ResNet-50 for RGB images.

A comparison among the original ResNet-50 network [16], the Upsampling-RFA [9], and our proposed techniques is presented in Figure 2. Initially, in Section IV-A, we proposed a handcrafted technique named Frequency Band Selection (FBS), where we manually select a subset of the most relevant DCT coefficients before feeding them to the network; Then in Section IV-B, we tested data-driven techniques to reduce the amount of input channels; Finally, in Section IV-C we explored the effects of reducing the amount of layers of the CNN combined with data-driven techniques to adapt the input size.

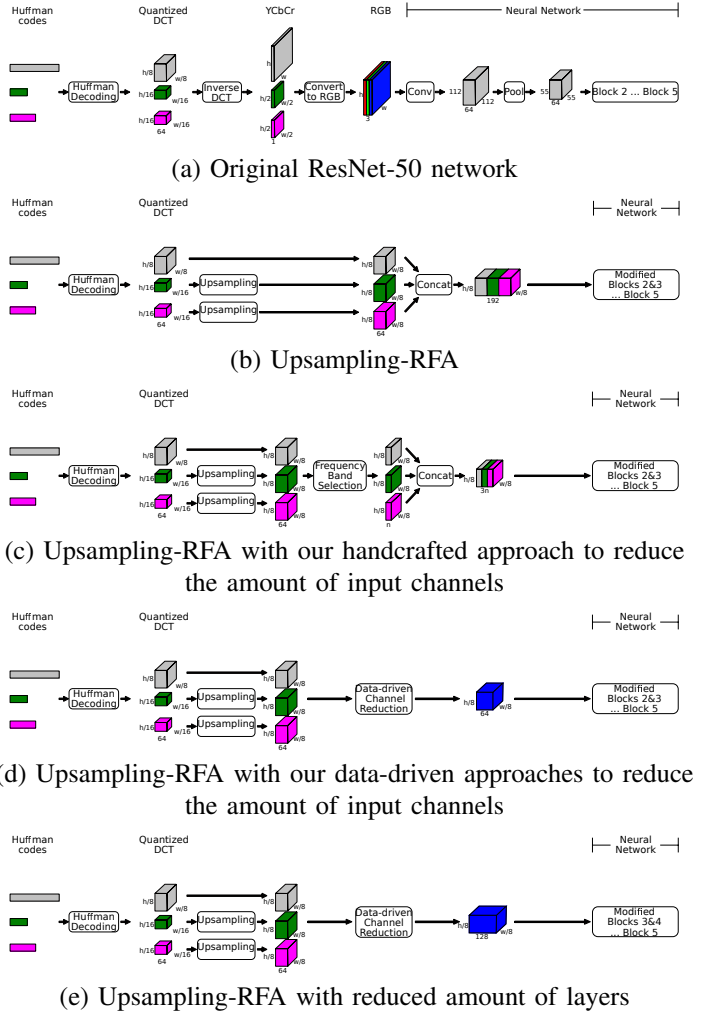


Fig. 2. Illustrations of (a) the original ResNet-50 network [16], (b) the Upsampling-RFA network proposed by Gueguen et al. [9], (c) our improved version with handcrafted and (d) data-driven techniques to reduce the amount of channels, and (e) our method to reduce the amount of layers with data-driven techniques to adapt the input.

#### A. Reducing the Number of Input Channels with a Hand-crafted Technique

To alleviate the computational complexity and the number of parameters, of the Upsampling-RFA [9], we proposed to use a Frequency Band Selection (FBS) technique to select the most relevant DCT coefficients before feeding them to the network. Since higher frequency information has little visual effect on the image, we retain the  $n$  lowest frequency coefficients and analyze how they impact the classification accuracy of the network.

For that, the second stage of the ResNet-50 network was changed to accommodate the amount of retained coefficients, i.e.,  $3n$  input channels. In this way, when FBS is set to  $n = 64$ , the network architecture is the same as Upsampling-RFA [9] and the number of output channels at the end of the second stage is equals to 256, while for  $n = 16$ , the number of output channels is the same amount of the original ResNet network [16], i.e., 64.

### B. Reducing the Number of Input Channels with Data-driven Techniques

The results obtained by the FBS technique proposed in Section IV-A indicates that reducing the number of channels in early stages of the network can be effective in reducing the computational costs of the network. For this reason, we decided to explore smarter strategies to make this reduction.

First, we reduce the number of input channels of the second stage to 64 but we kept the decreased strides at its early blocks, as proposed by Gueguen et al. [9]. To accommodate this amount of input channels, we change number of output channels of the second and third stages are changed to be the same as the original ResNet-50. Then, we evaluate different strategies to reduce the number of DCT inputs from 192 (i.e., 3 color components  $\times$  64 DCT coefficients) to 64.

Unlike the FBS, where the DCT inputs are discarded by hand potentially losing image information, these techniques take advantage of all DCT inputs and learn how to combine them in a data-driven fashion. For this, we evaluate three different approaches: (1) a linear projection (LP) of the DCT inputs (Section IV-B1), (2) a local attention (LA) mechanism (Section IV-B2), and (3) a cross channel parametric pooling (CCPP) (Section IV-B3).

1) *Linear projection (LP)*: The ResNet-50 network [16] have residual learning applied to every block of few stacked layers, given by Equation 1, where  $F()$  is the residual mapping to be learned by the  $i$ -th block of stacked layers,  $W_i$  are its parameters,  $x$  are the input data, and  $y$  are the output feature maps.

$$y = F(x, W_i) + x \quad (1)$$

The  $F() + x$  operation is executed by a shortcut connection and a element-wise addition, but their dimensions must be equal. When they are not, a  $W_s$  linear projection can be applied in order to match the dimension. As can be seen in Equation 2, assuming that  $x$  have  $n$  input features maps and  $W_s$  is a weight matrix of size  $m \times n$ , the product  $W_s \cdot x$  will output in  $m$  feature maps, where each one is a linear combination of all the  $n$  inputs from  $x$ .

$$y = F(x, W_i) + W_s \cdot x \quad (2)$$

We apply this linear projection to reduce the number of channels from 192 of the DCT inputs to 64 of the convolution block of the second stage. In this way, we consider the DCT inputs as a whole regardless the importance of each of their frequencies to the image content. Also, the skewness or kurtosis (shape) of their distribution is preserved by the linear transformation.

2) *Local attention (LA)*: Visual attention is the cognitive process where, given a natural scene, the most significant visual information is selected while other redundant information is filtered out, being an important mechanism for the human visual system [20]. Attention mechanics for CNNs can have many types of variants, like spatial, channel and self-attention, according to the dimensions of the input they focus. In the case of channel attention, importance weights are learned and attached to the input channels [32].

The local attention proposed by Luong et al. [34] is a soft attention mechanism used on the machine translation task to analyze a word with a small context window of adjacent words, learning attention maps which focus on relevant parts of the input information.

We adapt this mechanism to be used as channel attention for the DCT inputs in order to reduce the number of channels from 192 to 64. This is performed according to Equation 3, where  $x$  is an input with  $n$  features maps,  $r$  is its reshaped version partitioning it into  $m$  groups of  $\frac{n}{m}$  channels,  $W$  is a weight matrix of size  $m \times (\frac{n}{m})$ ,  $y$  is an output with  $m$  feature maps, and  $\odot$  is the Hadamard product.

$$\begin{aligned} r &= \text{reshape}\left(x, \left[m, \frac{n}{m}\right]\right) \\ s &= W \odot r \\ a_i &= \text{softmax}(s_i), \forall i \in \{1 \dots m\} \\ y_i &= a_i \cdot r_i, \forall i \in \{1 \dots m\} \end{aligned} \quad (3)$$

First, the input  $x$  is split into  $m$  partitions  $r = \{r_1, \dots, r_m\}$  with  $\frac{n}{m}$  features maps. Then, alignment scores  $s$  are obtained by computing the Hadamard product between  $W$  and  $r$ . For each partition  $i \in \{1 \dots m\}$ , alignment scores  $s_i$  are normalized by applying the softmax function, producing attention maps  $a_i$  which are used to amplify or attenuate the focus of the distribution of the input data  $r_i$ . Therefore, the feature map  $y_i$  outputted for the  $i$ -th partition is a linear combination of adjacent channels. In this way, we preserve information of the DCT spectrum for the entire range of frequencies.

3) *Cross Channel Parametric Pooling (CCPP)*: In a cross channel parametric pooling layer, a weighted linear recombination of the input features maps is performed and then passed though a rectifier linear unit (ReLU) [35]. Min Lin et al. [35] proposed to use a cascade of such layers to replace the usual convolution layer of a CNN, since they have enhanced local modeling and the capability of being stacked over each other. Formally, a cascaded cross channel parametric pooling is performed according to Equation 4 [35], where  $f_{i,j,k}^l$  stands for the output of the  $l$ -th layer,  $x_{i,j}$  is the input patch centered at the pixel  $(i, j)$ ,  $k$  is used to index the feature maps,  $W_{l,k}$  and  $b_{l,k}$  are, respectively, weights and biases of the  $l$ -th layer for the  $k$ -th filter, and  $N$  is the number of layers.

$$\begin{aligned} f_{i,j,k}^1 &= \max(0, W_{1,k}^T \cdot x_{i,j} + b_{1,k}) \\ &\vdots \\ f_{i,j,k}^N &= \max(0, W_{N,k}^T \cdot f_{i,j}^{N-1} + b_{N,k}) \end{aligned} \quad (4)$$

The cross channel parametric pooling is equivalent to a convolutional layer with a kernel size of  $1 \times 1$  [35], which is also know as a pointwise convolution [36], being capable of projecting the input feature maps into a new channel space, increasing or decreasing the amount of channels.

We used a cross channel parametric pooling layer to reduce the number of channels from 192 to 64. Similar to the linear projection, the individual importance of each DCT coefficient for the image content is also not taken into account. On the other hand, the non-linear properties of the ReLU activation encourages the model to learn sparse feature maps, making it less prone to overfitting.

### C. Reducing the Number of Layers

The Upsampling-RFA [9] skips the first stage of the original ResNet-50, feeding the DCT coefficients to the second stage, which is modified to accommodate the amount of input channels. In order to reduce the complexity and amount of parameters from the network even further, we analyze the effects of skipping the second, third, and fourth stages of the original ResNet-50, but maintaining the stride reduction proposed by Gueguen et al. [9] at the early blocks of the initial stage in which the DCT coefficients are provided as input.

Different from Gueguen et al. [9], we do not increase the number of input channels at the initial stages, since it would lead to a great increase on the computational complexity of the network. Instead, we keep them the same as the original ResNet-50, whose the number of input channels in the second, third, fourth, and fifth stages are 64, 128, 256, and 512, respectively.

To accommodate such amount of channels, the data-driven strategies presented in the previous section were used to decrease or increase the DCT inputs from 192 (i.e., 3 color components  $\times$  64 DCT coefficients) to the amount of input channels of the initial stage in which they are provided as input. Notice that the number of DCT coefficients is close to the number of input channels of the third stage, requiring a less drastic reduction than the one needed to feed them on the second stage. On the other hand, the expected inputs for the fourth and fifth stages have a greater amount of channels than the DCT inputs and, for this reason, they need to be scaled up, however preserving the salient features as the original data.

## V. EXPERIMENTAL PROTOCOL

All the experiments were executed on a machine equipped with a processor Intel Core i7 6850K 3.6 GHz, 64 GBytes of DDR4-memory, and 3 NVIDIA Titan Xp GPUs. The machine runs Ubuntu 18.04 LTS (kernel 5.0.0) and the ext4 file system. Our experiments were execute on the ImageNet dataset and a subset of it.

Since we did not had access to the original implementation, of Gueguen et al. [9] models, we re-implemented them following the specifications available and trained them from scratch. In order to make a fair comparison, we present the results of our networks trained from scratch, as well as the results obtained from models trained from other works, showing that the variance present in the training of the network, and small variations in training procedures can generate variance in the results obtained by these models.

In order to compare our approach with the state-of-the-art, we selected models that made similar alterations to the network architecture as our methods, attempting to reduce the amount of channels of the networks designed for DCT coefficients to make them more similar to the the original ResNet-50 for RGB images. For this reason, we did not include models like the ones based on the LC-RFA Thinner [9], since they have a smaller amount of channels than the original ResNet-50, although this modifications could also be applied to our methods.

Experiments were performed using the ResNet-50, Upsampling-RFA, Upsampling-RFA + FBS, Upsampling-RFA + LP, Upsampling-RFA + LA, Upsampling-RFA + CCPP and Upsampling-RFA + CCPP skipping the 1<sup>st</sup> and 2<sup>nd</sup> stages, batch size of 128, initial learning rate of 0.05, momentum of 0.9, and were trained for 120 epochs, reducing the learning rate by a factor of 10 every 30 epochs. All images were resized so the smallest side is 256 and the crop size is 224x224. Data augmentation with random crop and horizontal flip was used on the training phase, while on test, only a center crop was used.

Initially, we conducted ablation studies with our handcrafted approach on a subset of the ImageNet [37] dataset<sup>1</sup>. For that, 211 of the 1000 classes were taken from the ILSVRC12 dataset and then grouped into 12 classes, namely: ball, bear, bike, bird, bottle, cat, dog, fish, fruit, turtle, vehicle, sign. This subset is composed of 268,773 images and was split into a training set of 215,018 (80%) images and a test set of 53,755 (20%) images. Two classification difficulties were tested on this subset, fine-grained, where 211 out of 1,000 classes from the ILSVRC12 dataset were used, and coarse-grained, where these classes are grouped into 12 categories. Finally, We evaluated the classification accuracy of all our propose methods on the entire ImageNet dataset.

To compare the performance of the network on the image classification task, we used the accuracy metric. In order to compare the efficiency of the networks, we used the amount of trainable parameters, the number of floating point operations (measured in GFLOPs), inference time and the frames per second (FPS).

For measuring inference time, we used a single Titan XP GPU and followed Deguerre et al. [7] by doing 10 runs of 200 predictions with batch size of 8. The final inference times are the average over all runs. Following Gueguen et al. [9], we also loaded the data into the memory previously to the time measurements, but differently than these works, we loaded the JPEG compressed data, allowing us to analyze the effects of partially or fully decoding the images.

We divided inference time on data preprocessing time and the time for passing the data through the network. Data preprocessing time includes the time for fully or partially decoding the images, applying the necessary operations and loading them into the GPU memory. All images were center cropped previously to the execution of these experiment. FPS is calculated over the average total inference time. FPS from other works are also reported, but are not directly comparable to ours, since they use different GPU implementations and, in some cases, different experimental protocol to do the measurements.

## VI. EXPERIMENTAL RESULTS

This section presents the experimental results obtained in this work. Section VI-A presents preliminaries ablation studies conducted on a subset of the ImageNet dataset in order to

<sup>1</sup>The script for generating the ImageNet subset is available at <https://github.com/dusty-nv/jetson-inference/blob/master/tools/imagenet-subset.sh> (As of January, 2022)

investigate the effects of different channel selection strategies, image resolution, JPEG quality and classification task difficulty. Section VI-B shows the effects our proposed methods for reducing the number of input channels; Section VI-C shows the results of our experiments reducing the number of layers. Finally, Section VI-D presents a deeper analyses on the efficiency of the models, comparing inference time and FPS of the networks.

### A. Ablation Studies

Our ablation studies were conducted on a subset of the ImageNet dataset. The initial experiments had the objective of validating our handcrafted approach, the FBS technique, testing different coefficient ranges, image resolution and JPEG quality. For this, we evaluated our methods on the coarse grained classification difficulty of the subset.

We started by testing different ranges of DCT coefficients to analyse which one contain the most relevant information. For this, we selected 32 coefficients from each color channel with four different strategies: Selecting the lowest (coefficients 1 to 32), median (coefficients 17 to 48), highest (coefficients 33 to 64) and extremes frequencies (coefficients 1 to 16 and 49 to 64). The results can be seen in Table I.

TABLE I

COMPARISON OF CLASSIFICATION ACCURACY FOR USING DCT COEFFICIENTS FROM DIFFERENT FREQUENCY RANGES AS INPUT TO THE NETWORK ON THE COARSE GRAINED CLASSIFICATION TASK FROM THE IMAGENET SUBSET.

Approach	Accuracy
Lowest frequencies	94.53
Median frequencies	93.27
Highest frequencies	90.67
Extreme frequencies	94.12

The best performing strategy was selecting the lowest frequency coefficients, the second and third best were selecting the extreme and median frequencies, respectively, both including some coefficients from the lowest frequencies, while selecting only the highest frequencies was the worse strategy. These results indicate that our initial hypothesis, that higher frequency information has little visual effect on the image, was correct. For this reason, selecting the lowest frequency coefficients is the best strategy, and was used in all other experiments with the FBS method.

In our next experiment, we analysed the effects of different spatial resolution, as seen in Table II, where values inside parentheses are the number of input channels of each network. For this, we resized all the images to have their smallest side with 256, 128, 64, and 32 pixels and used the crop sizes of 224x224, 112x112, 56x56, and 28x28, respectively. As it can be seen, the reduction in the spatial resolution yielded a significant impact on the classification accuracy of all the networks, although the DCT-based ones were more affected, significantly reducing the accuracy.

We also analyzed the effect of reducing the quality setting used to encode JPEG images, as can be observed in Table III. All the networks were robust to this parameter, yielding a small

TABLE II

COMPARISON OF CLASSIFICATION ACCURACY (%) FOR THE ORIGINAL RESNET-50 WITH RGB INPUTS, THE UPSAMPLING-RFA AND ITS VARIANTS USING OUR FBS TECHNIQUE ON THE COARSE CLASSIFICATION TASK OF THE IMAGENET SUBSET WITH MULTIPLE IMAGE RESOLUTIONS.

Approach	Image Resolution			
	32	64	128	256
ResNet-50 (3x1) [16]	81.82	90.39	94.56	96.49
Upsampling-RFA (3x64) [9]	72.72	82.06	90.32	94.15
Upsampling-RFA + FBS (3x32)	71.83	82.22	90.78	94.53
Upsampling-RFA + FBS (3x16)	70.35	81.35	90.16	93.92

drop in accuracy, lower than 1% even for the worse quality setting.

TABLE III

COMPARISON OF CLASSIFICATION ACCURACY (%) FOR THE ORIGINAL RESNET-50 WITH RGB INPUTS, THE UPSAMPLING-RFA AND ITS VARIANTS USING OUR FBS TECHNIQUE ON THE COARSE CLASSIFICATION TASK OF THE IMAGENET SUBSET AND IMAGES WITH DIFFERENT JPEG QUALITIES.

Approach	JPEG Quality			
	25	50	75	100
ResNet-50 (3x1) [16]	95.78	95.98	96.09	96.49
Upsampling-RFA (3x64) [9]	93.84	94.02	94.50	94.15
Upsampling-RFA + FBS (3x32)	93.63	93.97	94.20	94.53
Upsampling-RFA + FBS (3x16)	92.69	93.26	93.66	93.92

In our last experiment with this subset, we considered both classification difficulties available, coarse and fine grained, and all our proposed methods to reduce the number of input channels, handcrafted and data-driven, as can be seen in Table IV

TABLE IV

COMPARISON OF CLASSIFICATION ACCURACY (%) FOR THE IMAGENET SUBSET WITH DIFFERENT CLASSIFICATION DIFFICULTY LEVELS WITH THE ORIGINAL RESNET-50 WITH RGB INPUTS, THE UPSAMPLING-RFA AND ITS VARIANTS USING OUR FBS AND DATA-DRIVEN CHANNEL REDUCTION TECHNIQUES ON THE IMAGENET SUBSET.

Approach	Classification Task	
	Fine (211 Classes)	Coarse (12 Classes)
ResNet-50 (3x1) [16]	76.28	96.49
Upsampling-RFA (3x64) [9]	70.28	94.15
Upsampling-RFA + FBS (3x32)	69.79	94.53
Upsampling-RFA + FBS (3x16)	68.12	93.92
Upsampling-RFA + LP (1x64)	70.08	93.17
Upsampling-RFA + LA (1x64)	69.15	94.23
Upsampling-RFA + CCPP (1x64)	70.09	94.85

All networks obtained a higher classification accuracy on the coarse grained task than on the fine grained task. This result can be attributed to fact that the fine grained has a higher amount of classes than the coarse grained, being a more challenging task.

For both tasks, the RGB-based network (ResNet-50) had better classification accuracy than the DCT-based ones (Upsampling-RFA variants). In the fine-grained task, the second best network was the Upsampling-RFA [9], which obtained a result 6% lower than the RGB.

In the coarse-grained task, all our data-driven techniques to reduce computational complexity were able to outperform the classification accuracy of the Upsampling-RFA, while at the same time, having lower computational complexity and amount of parameters. Among them, CCPP was the best, with accuracy only 1.64% lower than the RGB baseline. Our hand-crafted approach, when using 32 coefficients (Upsampling-RFA + FBS (3x32)) was also able to obtain better classification accuracy than the Upsampling-RFA, being 1.96% lower than the RGB.

### B. Effects of Reducing the Number of Input Channels

We evaluated the computational complexity, amount of parameters, frames per second and accuracy of both our handcrafted and data-driven networks on the entire ImageNet dataset, as it can be seen in Table V.

TABLE V

COMPARISON OF COMPUTATIONAL COMPLEXITY (GFLOPS), NUMBER OF PARAMETERS, FRAMES PER SECOND ON INFERENCE AND CLASSIFICATION ACCURACY FOR THE ORIGINAL RESNET-50 WITH RGB INPUTS AND NETWORKS USING DCT AS INPUT FOR IMAGE CLASSIFICATION ON THE IMAGENET DATASET.

Approach	GFLOPs	Params	FPS	Accuracy
<u>Gueguen et al. [9] training:</u>				
ResNet-50 (3x1)	3.86	25.6M	208	75.78
Upsampling-RFA (3x64)	5.40	28.4M	266	75.94
LC-RFA (3x64)	5.11	27.4M	267	75.92
Deconvolution-RFA (3x64)	5.39	28.4M	268	76.06
<u>Deguerre et al. [7] training:</u>				
ResNet-50 (3x1)	3.86	25.6M	324	74.73
LC-RFA (3x64)	5.11	27.4M	318	74.82
LC-RFA Y (1x64)	5.14	27.6M	329	73.25
Deconvolution-RFA (3x64)	5.39	28.4M	319	74.55
<u>Our training:</u>				
ResNet-50 (3x1)	3.86	25.6M	457	73.46
Upsampling-RFA (3x64)	5.40	28.4M	465	72.33
Upsampling-RFA + FBS (3x32)	3.68	26.2M	597	70.22
Upsampling-RFA + FBS (3x16)	3.18	25.6M	653	67.03
Upsampling-RFA + LP (1x64)	3.20	25.6M	554	69.62
Upsampling-RFA + LA (1x64)	3.20	25.6M	542	69.96
Upsampling-RFA + CCPP (1x64)	3.20	25.6M	555	69.73

The three models with the best classification accuracy were, respectively, the Deconvolution-RFA, Upsampling-RFA and LC-RFA trained by Gueguen et al. [9]. All these models use DCT coefficients as inputs, and were able to achieve better classification accuracy than the RGB baselines. The training of these networks made by Deguerre et al. [7] and us were able to obtain classification accuracy similar to the RGB, but did not surpass it. In general, when comparing the same models trained by different authors, the best accuracy were obtained by Gueguen et al. [9], followed by Deguerre et al. [7] and us, showing that small differences in procedures and training variance can affect the performance of these models.

The FPS obtained were also different for each work, since different hardware, batch size and other configurations were used. In Gueguen et al. [9] experiments and ours, all DCT models were able to obtain higher FPS than the RGB baseline, while for Deguerre et al. [7], the LC-RFA and Deconvolution-RFA obtained lower FPS than the RGB model by a small margin, 6 and 5 frames, respectively, achieving a similar inference speed.

For this reasons, in the remainder of this work, when multiple training results for the same network were available, we used ours to keep a fair comparison.

The Upsampling-RFA is faster than the base ResNet-50 duo to the time saved by only partially decoding the image and skipping the first stage of the original network, but the modifications made to accommodate DCT coefficients increased the computational complexity and number of parameters.

Among the DCT models trained by Gueguen et al. [9] and Deguerre et al. [7], the one with the best classification accuracy only increased it by 0.36% compared to their RGB baseline, while the one with lowest complexity increased it by 32.38% and had at least 1.8M more parameters. Also Deguerre et al. [7] LC-RFA and Deconvolution-RFA obtained similar but smaller FPS than the ResNet-50. This shows that even though there is a reduction on the cost of data prepossessing for these networks, the increase in the network cost can outweighs it, leading to a similar FPS.

In our experiments, the Upsampling-RFA gained only 8 FPS over the RGB base line, had a small drop in classification accuracy (around 1.13%), demanded an increase of approximately 39.9% in the computational complexity and 2.8M more parameters. Through the use of the FBS technique added to the Upsampling-RFA, it was possible to obtain more efficient models. Our Upsampling-RFA + FBS (3x32), that uses 32 coefficients per color channel, obtained a classification accuracy 3.24% lower and had 0.6M more parameters than our RGB baseline, but was able to reduce the complexity in 4.66% and gain 140 FPS. The Upsampling-RFA + FBS (3x16) presented a greater drop in classification accuracy of 6.43%, but also an even greater increases in efficiency, complexity was reduced in approximately 17.62%, 196 FPS were gained and the amount of parameters was approximately equal to the RGB baseline.

All our data-driven strategies obtained similar classification accuracy, computational complexity, number of parameters and FPS. Their amount of parameters were approximately the same as our RGB baseline, the complexity were approximately 17.1% lower and there was a increase between 85 and 98 FPS. LA performed slightly better, obtaining classification accuracy 3.5% lower than the RGB baseline, followed closely by CCPP and LP, that were 3.73% and 3.84% lower, respectively.

Compared to the FBS techniques, our data-driven strategies yielded a similar classification accuracy and FPS to Upsampling-RFA + FBS (3x32), while having a computational complexity similar to Upsampling-RFA + FBS (3x16) and the lowest amount of parameters from all the models presented this far, showing that the use of smarter strategies to learn how to reduce the number of input channels is a promising alternative.

### C. Effects of Reducing the Number of layers

In this section, we will present the results we obtained by our strategy to reduce the amount of layers from the Upsampling-RFA, proposed in Section IV-C.

When stages of the network are skipped, we need to decrease or increase the amount of inputs channels in order

to match the amount of channels expected at the initial stage in which they are provided as input. For this, we use the CCPP method, since the results for all the strategies presented in Section IV-B were similar. This strategy was chosen because it is commonly applied in CNNs in order to obtain channel-wise projections of the feature maps, like in depthwise separable convolutions [36]. Table VI presents the computational complexity and number of parameters of our Upsampling-RFA + CCPP skipping different stages.

TABLE VI  
COMPARISON OF COMPUTATIONAL COMPLEXITY (GFLOPS) AND NUMBER OF PARAMETERS FOR OUR UPSAMPLING-RFA + CCPP WHEN SKIPPING DIFFERENT STAGES.

Approach	GFLOPs	Params
Skip the first stage	3.20	25.6M
Skip the first and second stages	2.86	25.1M
Skip the first, second, and third stages	8.26	23.9M
Skip the first, second, third, and fourth stages	10.76	15.8M

As it can be seen, skipping the first and second stages was beneficial, reducing the computational complexity and number of parameters of the network. However, as more stages were skipped, although the number of parameters is decreased, the computational complexity is greatly increased. This is due to the fact that by removing the earlier stages of the network, we are feeding images with higher resolutions to the network, since those early stages would reduce the resolution of the image. For this reason and due to the decreased strides at the early blocks of the initial stage, the convolution operations have their cost increased though the network.

Due to those motives, skipping of the first and second stages is the only setting considered in the next experiments, since only it saves the computational costs of the network.

Table VII compares the computational complexity, number of parameters, frames per second and accuracy between our trained models presented previously and our strategy skip the first and second stages and use CCPP to accommodate the DCT inputs.

TABLE VII  
COMPARISON OF COMPUTATIONAL COMPLEXITY (GFLOPS), NUMBER OF PARAMETERS, FRAMES PER SECOND ON INFERENCE AND CLASSIFICATION ACCURACY ON THE IMAGENET DATASET FOR THE ORIGINAL RESNET-50 WITH RGB, NETWORKS DESIGNED FOR DCT, AND OUR STRATEGIES FOR REDUCING THE NUMBER OF INPUT CHANNELS AND LAYERS.

Approach	GFLOPs	Params	FPS	Accuracy
ResNet-50 (3x1)	3.86	25.6M	457	73.46
Upsampling-RFA (3x64)	5.40	28.4M	465	72.33
Upsampling-RFA + FBS (3x32)	3.68	26.2M	597	70.22
Upsampling-RFA + FBS (3x16)	3.18	25.6M	653	67.03
Upsampling-RFA + CCPP (1x64)	3.20	25.6M	555	69.73
Upsampling-RFA + CCPP + skipping 1 <sup>st</sup> and 2 <sup>nd</sup> stages (1x128)	2.86	25.1M	624	70.49

Skipping the first and second stages benefited not only computational costs of the network, but also its accuracy. It achieved the lowest amount of parameters and the second best FPS and classification accuracy among the DCT-based networks. It lost in classification accuracy to the Upsampling-RFA [9], whose FPS is lower and the computational complexity and number of parameters are considerable higher, and was

behind in FPS to the Upsampling-RFA + FBS (3x16), that had a lower classification accuracy. Compared to the original ResNet-50 the classification accuracy was only 1.13% lower, while there was a similar amount of parameters, a reduction of 25.91% in computational complexity and a gain of 167 FPS.

#### D. Analysing the Efficiency of the Models

Table VIII presents the results of our experiment to measure inference time and FPS. As can be seen, the data preprocessing time is lower than the network time, although it still has a considerable influence, being approximately 23.92% from the total inference time for the Upsampling-RFA. It is important to emphasize that such results are hardware and software dependent and thus may change according to the experimental setup.

TABLE VIII  
COMPARISON OF INFERENCE TIME AND FRAMES PER SECOND FOR THE ORIGINAL RESNET-50 WITH RGB, THE UPSAMPLING-RFA DESIGNED FOR DCT, AND OUR STRATEGIES FOR REDUCING THE NUMBER OF INPUT CHANNELS AND LAYERS. THE INFERENCE TIMES ARE AVERAGED FOR 10 RUNS OVER 25 BATCHES OF SIZE 8, AND  $\pm$ INDICATES THE STANDARD DEVIATION.

Approach	Average Inference Times (ms)			FPS
	Preprocessing	Network	Total	
ResNet-50 (3x1)	104.73 $\pm$ 24.58	333.13 $\pm$ 18.43	437.93 $\pm$ 37.18	457
Upsampling-RFA (3x64)	72.93 $\pm$ 9.77	356.89 $\pm$ 5.28	429.88 $\pm$ 9.26	465
Upsampling-RFA + FBS (3x32)	51.13 $\pm$ 16.41	283.76 $\pm$ 7.20	334.95 $\pm$ 22.18	597
Upsampling-RFA + FBS (3x16)	29.72 $\pm$ 10.41	276.39 $\pm$ 10.43	306.16 $\pm$ 14.84	653
Upsampling-RFA + LP (1x64)	80.65 $\pm$ 24.45	280.30 $\pm$ 10.59	361.01 $\pm$ 30.40	554
Upsampling-RFA + LA (1x64)	84.62 $\pm$ 20.68	284.64 $\pm$ 10.20	369.32 $\pm$ 19.52	542
Upsampling-RFA + CCPP (1x64)	79.55 $\pm$ 15.85	280.43 $\pm$ 10.96	360.04 $\pm$ 19.98	555
Upsampling-RFA + CCPP + skipping 1 <sup>st</sup> and 2 <sup>nd</sup> stages (1x128)	80.71 $\pm$ 17.06	239.73 $\pm$ 17.13	320.51 $\pm$ 29.97	624

The base RGB model, the ResNet-50, was the one with the higher data preprocessing time and overall prediction time, since it needs to fully decode the images before feeding them to the network.

By using DCT coefficients that can be obtained by partial decoding of the images, the Upsampling-RFA was able to reduce the data preprocessing time when compared to the ResNet-50 and even though the modifications made led to a higher network time, there was a small gain in FPS, since the decrease in data preprocessing time was more influential.

By using the FBS technique, the data preprocessing time was improved even further, together with a reduction in network time, generating big improvements on the FPS of the networks over the Upsampling-RFA and RGB baseline.

Our data-driven methods for reducing the amount of input channels also greatly improved the network time, but obtained similar data preprocessing time to the Upsampling-RFA. This indicates that the main source of reduction in time for the FBS methods is the discard of the unused DCT coefficients, reducing the cost of applying transformations on the data (like transposing, slicing and concatenation of tensors) and the time to load the data into the GPU. Our data-driven methods reduce the amount of channels after the aforementioned operations are executed, since they need to be incorporated to the network to be trained together, and for this reason, only obtain the gain in data preprocessing time for partially decoding the images. But they were able to get FPS similar to FBS (3x32), since their network time was also similar.

Skipping stages of the network obtained similar gains in data preprocessing time as the Upsampling-RFA since it also use our data-driven strategy to reduce the amount of input channels, but it had the best network time among the tested models, resulting on the second highest FPS, only behind the FBS (3x16).

The results we obtained here indicates that methods for improving the time of data preprocessing, like using network that work directly on compressed data and our FBS and data-driven techniques to reduce the amount of input channels are promising, since they reduce data preprocessing time as well as network time, being able to greatly speed-up the models.

Figure 3 compares the computational complexity, number of parameters, frames per second, and classification accuracy for the different networks evaluated on the ImageNet dataset. As it can be seen, although all networks have similar classification accuracy, the Upsampling-RFA significantly increased the computational complexity and number of parameters from the original ResNet-50, only leading to a small speed-up in relation to the RGB baseline. The use of the FBS technique was able to reduce the computational complexity and the number of parameters while keeping a similar classification accuracy and greatly increasing the FPS of the network.

Our data-driven approaches to reduce the amount of channels obtained similar classification accuracy to the FBS (3x32), FPS higher than the Upsampling-RFA but lower than the FBS (3x32) and a similar amount of parameters and computational complexity to the FBS (3x16).

And finally, by using a data-driven technique to reduce the amount of channels and skipping the 1<sup>st</sup> and 2<sup>nd</sup> stages, we obtained the DCT model with the best computational efficiency, having a good balance between classification accuracy and computational cost. It was able to obtain the second best accuracy and FPS and the lowest amount of parameters, having 0.5M less parameters than the our RGB baseline.

## VII. CONCLUSIONS

In this paper, we presented a study on CNNs designed to operate directly on frequency domain data, learning with DCT coefficients rather than RGB pixels. These information are readily available in the compressed representation of images, saving the high computational load of fully decoding the data and greatly speeding up the processing time, which is currently a big bottleneck of deep learning.

The starting point of our work was the state-of-the-art model proposed by Gueguen et al. [9], the Upsampling-RFA, which is a modified version of the ResNet-50 architecture [16]. Despite the speed-up obtained by partially decoding JPEG images, their architectural changes raised the computation complexity and the number of parameters of the network. To alleviate these drawbacks, we propose a Frequency Band Selection (FBS) technique to select the most relevant DCT coefficients before feeding them to the network.

Initially, we made ablation studies in a subset of ImageNet, where we showed that selecting the lowest frequency coefficients of the DCT was the best between all tested strategies, DCT models are sensitive to variations in image

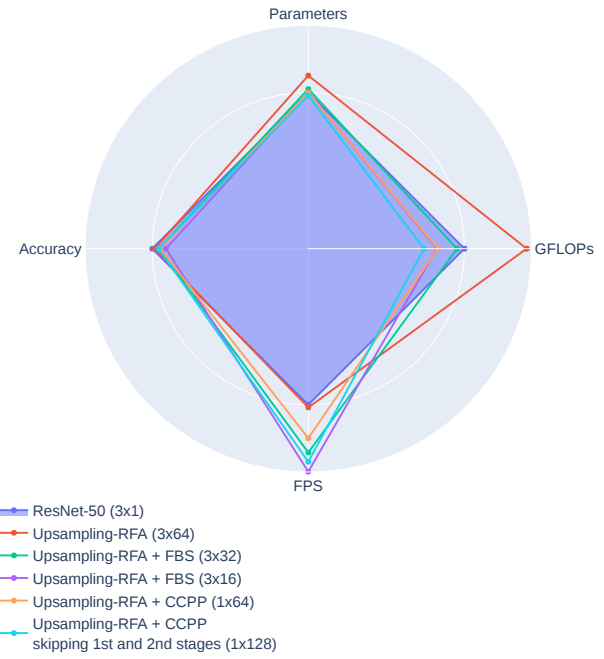


Fig. 3. Comparison of computational complexity, number of parameters, frames per second and classification accuracy from different networks for the image classification task on the ImageNet dataset. Values are shown in proportion to the ResNet-50.

resolution and robust to changes in JPEG quality. Our next experiments analyzed the impact on computational complexity and classification accuracy of the network when only the 64, 32, and 16 lowest frequency DCT coefficients of each color component were selected to be used as input in a handcrafted manner by our FBS method. The classification accuracy for the methods that use the FBS technique in the frequency domain can be similar to state-of-the-art methods, but its inference speed can be increased in up to 196 FPS.

Although the FBS technique is effective, relevant information from the DCT inputs are discarded. For this reason, we explored smart strategies to reduce the computational complexity without discarding useful information. Our results showed that learning how to combine all DCT inputs in a data-driven fashion was able to reduce computational complexity and the amount of parameters, reaching an classification accuracy and FPS similar to the FBS with 32 coefficients for each color channel.

Also, we found that skipping some stages of the network is beneficial, leading to model with the best balance between classification accuracy, FPS and amount of parameters, proving to be an efficient strategy.

As future work, we intend to evaluate other smart strategies to reduce computational complexity of the network. We also plan to extend our approach for video classification using 3D network architectures, like Res3D [38] or I3D [39]. Finally, we intend to evaluate our approach in large-scale datasets, like Kinetics [40], and in other applications.

## ACKNOWLEDGMENT

This research was supported by the FAPESP-Microsoft Research Virtual Institute (grant 2017/25908-6) and the Brazilian National Council for Scientific and Technological Development - CNPq (grant 314868/2020-8). We gratefully acknowledge the support of NVIDIA Corporation with the donation of the Titan Xp GPU used for this research.

## REFERENCES

- [1] B. Deguerre, C. Chatelain, and G. Gasso, "Fast object detection in compressed JPEG images," in *IEEE Intelligent Transportation Systems Conference (ITSC'19)*, 2019, pp. 333–338.
- [2] Y. Li, S. Gu, L. V. Gool, and R. Timofte, "Learning filter basis for convolutional neural network compression," in *Proceedings of the IEEE International Conference on Computer Vision*, 2019, pp. 5623–5632.
- [3] L. Liu, S. Zhang, Z. Kuang, A. Zhou, J.-H. Xue, X. Wang, Y. Chen, W. Yang, Q. Liao, and W. Zhang, "Group fisher pruning for practical network compression," in *International Conference on Machine Learning*. PMLR, 2021, pp. 7021–7032.
- [4] M. Ehrlich and L. S. Davis, "Deep residual learning in the JPEG transform domain," in *IEEE International Conference on Computer Vision (ICCV'19)*, 2019, pp. 3484–3493.
- [5] G. Ding, S. Zhang, Z. Jia, J. Zhong, and J. Han, "Where to prune: Using LSTM to guide data-dependent soft pruning," *IEEE Transactions on Image Processing*, vol. 30, pp. 293–304, 2020.
- [6] A. Marchisio, M. A. Hanif, F. Khalid, G. Plastiras, C. Kyrikou, T. Theοcharides, and M. Shafique, "Deep learning for edge computing: Current trends, cross-layer optimizations, and open research challenges," in *IEEE Computer Society Annual Symposium on VLSI (ISVLS'19)*, 2019, pp. 553–559.
- [7] B. Deguerre, C. Chatelain, and G. Gasso, "Object detection in the DCT domain: is luminance the solution?" in *25th International Conference on Pattern Recognition, ICPR 2020, Virtual Event / Milan, Italy, January 10-15, 2021*. IEEE, 2021, pp. 2627–2634. [Online]. Available: <https://doi.org/10.1109/ICPR48806.2021.9412998>
- [8] M. Ehrlich, L. Davis, S.-N. Lim, and A. Shrivastava, "Analyzing and Mitigating JPEG Compression Defects in Deep Learning," in *2021 IEEE/CVF International Conference on Computer Vision Workshops (ICCVW)*, 2021, pp. 2357–2367.
- [9] L. Gueguen, A. Sergeev, B. Kadlec, R. Liu, and J. Yosinski, "Faster neural networks straight from JPEG," in *Annual Conference on Neural Information Processing Systems (NIPS'18)*, 2018, pp. 3937–3948.
- [10] S.-Y. Lo and H.-M. Hang, "Exploring semantic segmentation on the DCT representation," in *Proceedings of the ACM Multimedia Asia*, 2019, pp. 1–6.
- [11] K. Xu, M. Qin, F. Sun, Y. Wang, Y.-K. Chen, and F. Ren, "Learning in the Frequency Domain," in *Proceedings of the IEEE/CVF Conference on Computer Vision and Pattern Recognition*, 2020, pp. 1740–1749. [Online]. Available: <https://github.com/PSCLab-ASU/Learning-in-the-Frequency-Domain>
- [12] M. Ehrlich, L. Davis, S.-N. Lim, and A. Shrivastava, "Quantization Guided JPEG Artifact Correction," in *Proceedings of the European Conference on Computer Vision*. Springer, 2020.
- [13] S. F. Santos, N. Sebe, and J. Almeida, "CV-C3D: action recognition on compressed videos with convolutional 3d networks," in *SIBGRAPI – Conference on Graphics, Patterns and Images (SIBGRAPI'19)*, 2019, pp. 24–30.
- [14] S. F. Santos and J. Almeida, "Faster and accurate compressed video action recognition straight from the frequency domain," in *SIBGRAPI – Conference on Graphics, Patterns and Images (SIBGRAPI'20)*, 2020, pp. 62–68.
- [15] Y. Tang, X. Zhang, X. Hu, S. Wang, and H. Wang, "Facial expression recognition using frequency neural network," *IEEE Transactions on Image Processing*, vol. 30, pp. 444–457, 2020.
- [16] K. He, X. Zhang, S. Ren, and J. Sun, "Deep residual learning for image recognition," in *IEEE International Conference on Computer Vision and Pattern Recognition (CVPR'16)*, 2016, pp. 770–778.
- [17] S. F. Santos, N. Sebe, and J. Almeida, "The good, the bad, and the ugly: Neural networks straight from jpeg," in *IEEE International Conference on Image Processing (ICIP'20)*, 2020, pp. 1896–1900.
- [18] K. Delac, M. Grgic, and S. Grgic, "Face recognition in JPEG and JPEG2000 compressed domain," *Image Vision Computing*, vol. 27, no. 8, pp. 1108–1120, 2009.
- [19] P. Poursistan, H. Nezamabadi-pour, R. A. Moghadam, and M. Saeed, "Image indexing and retrieval in JPEG compressed domain based on vector quantization," *Mathematical and Computer Modelling*, vol. 57, no. 5–6, pp. 1005–1017, 2013.
- [20] Y. Fang, Z. Chen, W. Lin, and C.-W. Lin, "Saliency detection in the compressed domain for adaptive image retargeting," *IEEE Transactions on Image Processing*, vol. 21, no. 9, pp. 3888–3901, 2012.
- [21] J. Almeida, N. J. Leite, and R. S. Torres, "Comparison of video sequences with histograms of motion patterns," in *IEEE International Conference on Image Processing (ICIP'11)*, 2011, pp. 3673–3676.
- [22] ———, "VISON: VIdeo Summarization for ONline applications," *Pattern Recognition Letters*, vol. 33, no. 4, pp. 397–409, 2012.
- [23] X. Wang, K. Yu, S. Wu, J. Gu, Y. Liu, C. Dong, Y. Qiao, and C. Change Loy, "EsrGAN: Enhanced super-resolution generative adversarial networks," in *Proceedings of the European Conference on Computer Vision (ECCV) Workshops*, 2018, pp. 0–0.
- [24] Z. Wang, A. C. Bovik, H. R. Sheikh, and E. P. Simoncelli, "Image quality assessment: from error visibility to structural similarity," *IEEE transactions on image processing*, vol. 13, no. 4, pp. 600–612, 2004.
- [25] S.-Y. Lo, H.-M. Hang, S.-W. Chan, and J.-J. Lin, "Efficient dense modules of asymmetric convolution for real-time semantic segmentation," in *Proceedings of the ACM Multimedia Asia*, 2019, pp. 1–6.
- [26] E. Jang, S. Gu, and B. Poole, "Categorical reparameterization with gumbel-softmax," *arXiv preprint arXiv:1611.01144*, 2016.
- [27] G. Tucker, A. Mnih, C. J. Maddison, D. Lawson, and J. Sohl-Dickstein, "Rebar: low-variance, unbiased gradient estimates for discrete latent variable models," *Annual Conference on Neural Information Processing Systems (NIPS'17)*, pp. 2624–2633, 2017.
- [28] C. J. Maddison, A. Mnih, and Y. W. Teh, "The concrete distribution: A continuous relaxation of discrete random variables," *Proceedings of the international conference on learning Representations*, 2017.
- [29] W. Liu, D. Anguelov, D. Erhan, C. Szegedy, S. E. Reed, C.-Y. Fu, and A. C. Berg, "SSD: single shot multibox detector," in *European Conference on Computer Vision (ECCV'16)*, 2016, pp. 21–37.
- [30] J. Li, Y. Wang, H. Xie, and K.-K. Ma, "Learning a single model with a wide range of quality factors for jpeg image artifacts removal," *IEEE Transactions on Image Processing*, vol. 29, pp. 8842–8854, 2020.
- [31] P. Chen, W. Yang, M. Wang, L. Sun, K. Hu, and S. Wang, "Compressed Domain Deep Video Super-Resolution," *IEEE Transactions on Image Processing*, vol. 30, pp. 7156–7169, 2021.
- [32] Z. Qin, P. Zhang, F. Wu, and X. Li, "Fcanet: Frequency channel attention networks," in *Proceedings of the IEEE/CVF International Conference on Computer Vision*, 2021, pp. 783–792.
- [33] L. Hanzo, P. Cherriman, and J. Streit, *Video Compression and Communications: From Basics to H.261, H.263, H.264, MPEG4 for DVB and HSDPA-Style Adaptive Turbo-Transceivers*, 2nd ed. Chichester, SXW, UK: John Wiley & Sons, 2007.
- [34] M.-T. Luong, H. Pham, and C. D. Manning, "Effective approaches to attention-based neural machine translation," in *Proceedings of the 2015 Conference on Empirical Methods in Natural Language Processing*, 2015, pp. 1412–1421.
- [35] M. Lin, Q. Chen, and S. Yan, "Network in network," *arXiv preprint arXiv:1312.4400*, 2013.
- [36] F. Chollet, "Xception: Deep learning with depthwise separable convolutions," in *CVPR*, 2017, pp. 1251–1258.
- [37] O. Russakovsky, J. Deng, H. Su, J. Krause, S. Satheesh, S. Ma, Z. Huang, A. Karpathy, A. Khosla, M. S. Bernstein, A. C. Berg, and F.-F. Li, "Imagenet large scale visual recognition challenge," *International Journal of Computer Vision*, vol. 115, no. 3, pp. 211–252, 2015.
- [38] D. Tran, J. Ray, Z. Shou, S.-F. Chang, and M. Paluri, "Convnet architecture search for spatiotemporal feature learning," *CoRR*, vol. abs/1708.05038, 2017.
- [39] J. Carreira and A. Zisserman, "Quo vadis, action recognition? A new model and the kinetics dataset," in *IEEE International Conference on Computer Vision and Pattern Recognition (CVPR'17)*, 2017, pp. 4724–4733.
- [40] W. Kay, J. Carreira, K. Simonyan, B. Zhang, C. Hillier, S. Vijayanarasimhan, F. Viola, T. Green, T. Back, P. Natsev, M. Suleyman, and A. Zisserman, "The kinetics human action video dataset," *CoRR*, vol. abs/1705.06950, 2017.